

Research Paper

Single-cell transcriptional profiling in osteosarcoma and the effect of neoadjuvant chemotherapy on the tumor microenvironment

Xiao-yu He^a, Liu-yi Que^a, Fan Yang^a, Yi Feng^b, Dong Ren^a, Xiang Song^{a,*}

^a Department of Oncology, Second Hospital of Shanxi Medical University, Taiyuan, Shanxi 030001, China

^b Department of Orthopedic Surgery, Second Hospital of Shanxi Medical University, Taiyuan, Shanxi 030001, China

HIGHLIGHTS

- The 9 cell types were identified, including fibroblasts, myeloid cells, osteoblasts, tumor-infiltrating lymphocytes (TILs), osteoclasts, proliferative osteoblasts, pericytes, endothelial cells, and B cells.
- After chemotherapy treatment, proportions of myeloid cells and TILs decreased in OS, while the number of osteoblasts increased.
- The study demonstrates the relationship between osteoclasts and osteosarcoma development.

ARTICLE INFO

Keywords:

Osteosarcoma
scRNA-seq
Tumor microenvironment
Tumor-infiltrating lymphocytes
Myeloid cells

ABSTRACT

Osteosarcoma (OS), a malignant tumor, originates from the bone marrow. Currently, treatment for OS remains limited, making it urgent to understand the immune response in the tumor microenvironment of patients with OS. A comprehensive bioinformatics analysis was performed, including cell clustering subgroups, differential expression genes screening, proposed temporal order, and genomic variant analysis on single-cell RNA-sequencing data, from ten pre-chemotherapy patients and eleven post-chemotherapy patients. Subsequently, we analyzed the differentiation trajectories of osteoblasts, osteoclasts, fibroblasts, myeloid cells, and tumor-infiltrating lymphocytes (TILs) in detail to compare the changes in cell proportions and differential genes pre- and post-chemotherapy. The nine cell types were identified, including fibroblasts, myeloid cells, osteoblasts, TILs, osteoclasts, proliferative osteoblasts, pericytes, endothelial cells, and B cells. Post-chemotherapy treatment, the proportions of myeloid cells and TILs in OS were declined, while the number of osteoblasts was elevated. Besides, a decrease was observed in CD74, FTL, FTH1, MT1X and MT2A, and an increase in PTN, COL3A1, COL1A1, IGFBP7 and FN1. Meanwhile, EMT, DNA repair, G2M checkpoint, and E2F targets were highly enriched post-chemotherapy. Furthermore, there was a down-regulation in the proportions of CD14 monocytes, Tregs, NK cells and CD1C-/CD141-DCs, while an up-regulation was observed in the proportions of SELENOP macrophages, IL7R macrophages, COL1A1 macrophages, CD1C DCs, CD4+ T cells and CD8+ T cells. Overall, these findings revealed changes in the tumor microenvironment of OS post-chemotherapy treatment, providing a new direction for investigating OS treatment.

1. Introduction

Osteosarcoma (OS) is a malignant tumor originating from the bone marrow, characterized by the formation of bone-like tissue or bone by tumor cells [1,2]. OS is not common, and there are approximately 750–900 new cases annually in the USA. Of them, approximately 400 cases occur in children and adolescents under the age of 20 [3]. Despite its rarity, OS is the most common primary bone malignancy in children

and adolescents and one of the fifth most common malignancies in adolescents aged 15–19 years [4]. Most OS occurs in the epiphysis of long bones. Notably, two-thirds of such tumors occur in the distal femur, followed by the proximal tibia (accounting for 10% of OS) [5]. Besides, 85% of patients present with localized lesions. Among those who develop metastases, 74% are affected only by pulmonary metastases, 9% solely by bone metastases, and 8% by bone and lung metastases. In adults over 65 years of age, there is a second peak in the incidence of OS

* Corresponding author.

E-mail address: songxiangeryuan@163.com (X. Song).

<https://doi.org/10.1016/j.jbo.2024.100604>

Received 11 September 2023; Received in revised form 28 April 2024; Accepted 29 April 2024

Available online 8 May 2024

2212-1374/© 2024 The Author(s). Published by Elsevier GmbH. This is an open access article under the CC BY-NC license (<http://creativecommons.org/licenses/by-nc/4.0/>).

due to secondary cancers and Paget's disease, with about 4.2 new cases per million per year [6].

Before the use of chemotherapeutic drugs, 80–90 % of patients with OS are controlled, but their prognosis is poor due to metastasis. After multidisciplinary therapy, two-thirds of patients with non-metastatic limb OS can achieve long-term survival, 50 % of patients with localized pulmonary metastases can be cured, and the recurrence-free survival for patients with extensive pulmonary metastases is 25 % [7,8]. To date, however, treatment for OS remains limited. It is urgent to understand the immune response in the tumor microenvironment (TME) of patients with OS to develop more effective and targeted therapies, thereby improving the prognosis of patients with OS [9].

At the turn of the century, it is possible to understand the pathogenesis of OS based on the well-annotated tissue libraries and more extensive comprehensive molecular profiling techniques. The detection of various common genetic alterations was found in OS, such as tumor protein 53 translocation and retinoblastoma protein 1 deletion, which can reduce the expression of key tumor suppressor proteins. Therefore, the detection combined with biomarker-based screening for clinical trials may increase the proportion of the population benefiting from OS [10]. Cellular differentiation of the mesenchymal lineage is another feature of OS, which maintains consistent expression of many cell-surface molecules. Hence, novel antibody-based cellular therapeutic approaches broaden the range of possible therapeutic targets for OS. The use of traditional transcriptome sequencing approaches is conducted in mixed cell populations, and their use is limited by genomic heterogeneity and the low quantity of available biological material [11]. For tumor cells, cells isolated from the same individual or cell line exhibit high heterogeneity, with often varied genomes that are difficult to decode using traditional bulk sequencing methods. Single-cell RNA sequencing (scRNA-seq) technology can make up for the shortcomings of traditional bulk genome sequencing methods, allowing highly specific studies of complex and diverse biological phenomena [12].

In this study, we conducted single-cell transcriptome sequencing of cancer tissues from four patients with OS and combined with scRNA-seq data from two Gene Expression Omnibus (GEO) datasets. Such processes identified nine major cell clusters and compared the effects of chemotherapeutic drugs on cell subtypes. This study deepens the understanding of the molecular characteristics of OS cells and may provide new ideas for future therapeutic approaches.

2. Method

2.1. Single-cell RNA sequencing dataset source

This study was approved by the Ethics Committee of the Second Hospital of Shanxi Medical University (2022YX NO.168) and complied with all relevant ethical regulations. All four patients were diagnosed with OS according to the NCCN Clinical Practice Guidelines (<https://www.nccn.org/>). All patients with OS underwent surgical treatment, followed by specimen collection for scRNA-seq analysis. The written informed consent was provided by all patients with OS. Surgical or biopsy specimens from 4 patients with OS were used for scRNA-seq analysis, and the clinical information of these patients was collected. The scRNA-seq information for GSE152048 (11 OS tissues) [13] and GSE162454 (6 OS tissues) [12] was obtained from the GEO database (<https://www.ncbi.nlm.nih.gov/geo/>). Of them, the OS biopsies were included.

2.2. Sample preparation and cell isolation for scRNA-seq

Fresh tumor lesions were preserved in MACS® Tissue Storage Solution (Miltenyi, USA) and processed on ice within 30 min after surgery. Specimens were rinsed three times with Hanks' Balanced Salt Solution and cut into small 1–2 mm pieces. Then, these pieces were digested with 2 ml of GEXSCOPE™ Tissue Dissociation Solution (Singleron) at 37 °C

for 15 min with continuous stirring. After digestion, the samples were filtered through a 40 µm sterile filter and centrifuged at 800 × g for 5 min. Subsequently, the supernatant was discarded and the cell pellet was suspended in 1 mL of phosphate-buffered saline (PBS; HyClone, USA). To remove the red blood cells, 2 mL of GEXSCOPE™ red blood cell lysis buffer (Singleron) was added, and cells were incubated at 25 °C for 10 min. The solution was then resuspended in PBS by centrifugation at 500 × g for 5 min. Samples were stained with trypan blue (Sigma, USA) and cell viability was assessed using a microscope (ZEISS, Germany).

Cells capture and cDNA synthesis were performed using Chromium Next GEM Automated Single Cell 3' Library and Gel Bead Kit v3.1 (10 × Genomics, cat#1000075, Pleasanton, CA, USA) and Chromium Single Cell B Chip Kit (10 × Genomics, cat#1000074, Pleasanton, CA, USA). The cell suspension (300–600 living cells per microliter determined by CountStar Rigel S2 Fluorescence cell analyzer) was loaded into a Chromium single cell controller (10 × Genomics, Pleasanton, CA, USA) to generate single-cell gel beads in the emulsion according to the operation manual. In short, single cells were suspended in PBS containing 0.04 % bovine serum albumin. Each channel was supplemented with about 6,000 cells. The captured cells were lysed to release RNA. Subsequently, the RNA was barcoded during the reverse transcription process. Approximately 3,000 target cells were estimated to be recovered.

Reverse transcription was performed on an S1000™ Touch Thermal Cycler (Bio-Rad, Hercules, CA, USA) at 53 °C for 45 min, followed by 85 °C for 5 min, and maintained at 4 °C. After generation, the cDNA was amplified, and quality assessment was carried out using an Agilent 4200 (performed by USBAY Biotechnology, Beijing, China). According to the instructions of manufacture, the scRNA-seq libraries were constructed using Chromium Next GEM Automated Single Cell 3' Library and Gel Bead Kit v3.1. Ultimately, the libraries were sequenced using an Illumina NovaSeq6000 sequencer (Illumina, San Diego, CA, USA). The sequencing depth was at least 100,000 reads per cell with a pair-end 150 bp (PE150) reading strategy (performed by USBAY Biotechnology, Beijing, China).

2.3. ScRNA-seq data quality control

Seurat package (version 4.1.0) in R was used to process and analyze the initial gene expression matrix. The conditions set were that the number of genes in the cells exceeded 500, the RNA count per cell was over 4000, and the mitochondrial read was less than 20 %. After filtering, the expression matrix was normalized using the \ln transformation [$\ln(\text{CPM} + 1)$] through the `NormalizeData` function in the Seurat package. Then, principal component analysis was performed using `RunPCA` with highly variable genes as input. Clustering was performed using a graph-based clustering algorithm and visualized using the `Run t-distributed stochastic neighbor embedding (t-SNE)` function in the Seurat package. Data integration was conducted using the canonical correlation analysis (CCA) in the Seurat package to deal with batch effects among different scRNA-seqs [14]. The parameters (`SelectIntegrationFeatures` and `FindClusters`) were utilized for CCA, and the 2000 most variable genes and the top 20 correlation vectors were selected.

2.4. Cell clustering and annotation

Wilcoxon test was applied to find the highly expressed genes in each cluster with the screening criteria of $p < 0.05$ and $|\log_2(\text{fold change (FC)})| \geq 1$. The top 10 highly expressed genes were then selected as marker genes for the cluster. We referred to the literature [13,15,16] and combined it with the single cell annotation website (CellMarker: <https://biocc.hrbmu.edu.cn/CellMarker/> [17]; PanglaoDB: <https://panglaoDB.se/index.html> [18]) for cell annotation.

2.5. Screening for differentially expressed genes

The DEGs pre- and post-chemotherapy were calculated by Seurat's

functions FindMarkers to explore differential expression genes (DEGs) among different cell subpopulations. The screening criteria were as follows: $p < 0.05$, $|\log_2(\text{FC})| \geq 1$. The results of the analysis were used for subsequent analysis.

2.6. Single-cell pseudotime trajectory analysis

Based on the results analyzed with Seurat, single-cell trajectory analysis was performed using the monocle2 package [19]. This analysis can infer the differentiation trajectories of cells during development or the evolution of cell subtypes, and is used more frequently in development-related studies. In this study, the individual cells were sorted in the proposed time based on the expression patterns of key genes. Notably, we stimulated the dynamic changes that occur during cell development as the proposed time progresses, thus facilitating the cell differentiation trajectories and key gene changes in patients with OS pre- and post-chemotherapy.

2.7. Single-cell copy-number variation assessment

The inferCNV package was utilized for the copy-number variation (CNV) assessment in each cell. Immune cells were used as a reference to calculate the CNVs of osteoblasts and fibroblasts. Parameters used in the inferCNV included noise reduction, the default Hidden Markov Model settings and a cut-off value of 0.1. To reduce false positive CNV calls, a default Bayesian latent mixture model was used to identify the posterior probability of CNV variation in each cell, with a default value of 0.5 as the threshold [16].

2.8. Gene set variation analysis

Gene set variation analysis (GSVA) was performed using the GSVA package in R to assess the pathway activity of each cell population pre- and post-chemotherapy. The pathway activity dataset used in the study was derived from the hallmark gene sets in the Molecular Signatures Database (<https://www.gsea-msigdb.org/gsea/msigdb>) [20].

2.9. Statistical analysis

All statistical analyses were performed using the R software, version 4.1.2 (<https://www.rproject.org>). $P < 0.05$ was considered statistical significance.

3. Results

3.1. The osteosarcoma microenvironment contains multiple cell subtypes, and differences exist among different cell subtypes pre- and post-chemotherapy

The scRNA-seq analysis was performed on cell specimens from four OS surgical/puncture specimens (Fig. 1A). Meanwhile, we obtained the scRNA-seq public data for 11 OS samples (GSE152048) and 6 OS samples (GSE162454) from GEO database. Then, the scRNA-seq data were divided into two groups: pre-chemotherapy ($n = 10$) and post-chemotherapy ($n = 11$), and the effect of chemotherapy on each cell population in patients with OS was analyzed. Afterward, CCA was used to integrate scRNA-seq from 21 patients with OS, and after quality control filtering, a total of 134,579 cells were obtained from 21 tumor samples. Based on the cell surface marker, the cells were classified into nine types: fibroblasts (COL1A1, cluster 0), myeloid cells (LYZ, cluster 1), osteoblasts (ACP5, cluster 2), TIL (CD3D, cluster 3), osteoclasts (CTSK, cluster 4), proliferative osteoblasts (TOP2A, cluster 5), pericytes (RGS5, cluster 6), endothelial cells (PECAM1, cluster 7), and B cells (MZB1, cluster 8) (Fig. 1B–D). We compared the differences in the proportions of each cell pre- and post-chemotherapy in patients with OS. Most notably, the proportions of myeloid cells and TILs were decreased

after treatment, while the number of osteoblasts and proliferative osteoblasts were increased (Fig. 1E, Supplementary Fig. 1).

3.2. Osteogenic cell structure in osteosarcoma TME and its effect by chemotherapy

Cell clusters of highly expressing IBSP cells were defined as osteoblasts, followed by the analysis with t-SNE. We found seven subpopulations with a total of 26,158 osteoblasts, including NEAT1 osteoblasts (12,557), TOP2A osteoblasts (4,291), RRM2 osteoblasts (3,433), IBSP osteoblasts (2,910), CD74 osteoblasts (2,241), MZB1 osteoblasts (397) and TPSB2 osteoblasts (329) (Fig. 2A–B). The chromosomal CNV of each cell subtype was calculated and identified in this study based on the transcriptome of inferCNV to distinguish the malignancy of different subtypes of osteoblasts. The results revealed that osteoblasts exhibited different levels of CNV, with CD74 osteoblasts showing a reduction in CNV on chromosome 1 and RRM2 osteoblasts presenting an increase in CNV on chromosome 8 (Fig. 2C). To further clarify the effect of chemotherapy on osteoblasts, the pseudotime trajectory analysis of osteoblasts was performed and a dendrogram of osteoblasts differentiation trajectories was constructed. Compared to pre-chemotherapy, CD74 osteoblasts and TPSB2 osteoblasts differentiated into RRM2 osteoblasts, NEAT1 osteoblasts and TOP2A osteoblasts post-chemotherapy. With the evolution of osteoblasts in chemotherapy trajectory before and after treatment, we intersected the monoclonal evolution genes with differential genes pre- and post-chemotherapy (Fig. 2D). Post-chemotherapy, CD74, FTL, FTH1, MT1X and MT2A were down-regulated, while PTN, COL3A1, COL1A1, IGFBP7 and FN1 were up-regulated (Fig. 2E, Supplementary Fig. 2). We compared the osteoblasts in different fractions pre- and post-chemotherapy, and similarly found that the proportions of NEAT1 osteoblasts, TOP2A osteoblasts and RRM2 osteoblasts were increased post-chemotherapy (Fig. 2E).

A GSVA analysis was performed to further reveal the effect of chemotherapy on the biological role of osteoblasts. We found that post-chemotherapy, there was a significant enrichment in epithelial-mesenchymal transition, DNA repair, glycolysis, MYC targets v1, G2M checkpoint, apical junction, coagulation, oxidative phosphorylation, E2F targets, angiogenesis and myogenesis. Notably, a remarkable decrease was observed in TNF- α signaling via NF- κ B, inflammatory response, IL6/Jak/Stat3 signaling, interferon gamma response, allograft rejection, IL2-STAT5 signaling, KRAS signaling DN, interferon-alpha response, estrogen response early, UV response up and P53 pathway (Fig. 2F).

3.3. Increased proportion of MMP9-expressing osteoclasts in osteosarcoma suggests a tumor-promoting effect

Osteoclasts, a kind of multinucleate cells, play a unique role in bone resorption and are significantly involved in bone destruction. Conventional OS can induce osteoclastogenesis by secreting osteoclast-inducing factors and targeted therapy against osteoclasts can control osteoclast differentiation and bone resorption, potentially offering a new approach for OS treatment. Osteoclasts were classified by OS scRNA-seq into CTSK osteoclasts (3,943), LGALS9 osteoclasts (2,218), CD74 osteoclasts (1,830), CCL3A1 osteoclasts (1,499), HMGB2 osteoclasts (1,314) (Fig. 3A). Post-chemotherapy, 91 DEGs were up-regulated and 237 DEGs were down-regulated in osteoclasts, with the most significant differences observed in the top 10 genes: TCIRG1, ACP5, JDP2, RGS10, MMP9, CCL3L1, CCL4L2, CCL3, CCL4, and IL1B. Notably, MMP9 was highly expressed in CTSK osteoclasts, LGALS9 osteoclasts and COL3A1 osteoclasts, indicating that targeting MMP9 might be a new direction for OS treatment (Fig. 3B–C). Subsequent proposed time series analysis uncovered that chemotherapy decreased the proportions of HMGB2 osteoclasts and increased the proportions of CTSK osteoclasts, LGALS9 osteoclasts and COL3A1 osteoclasts (Fig. 3D–F, Supplementary Fig. 3).

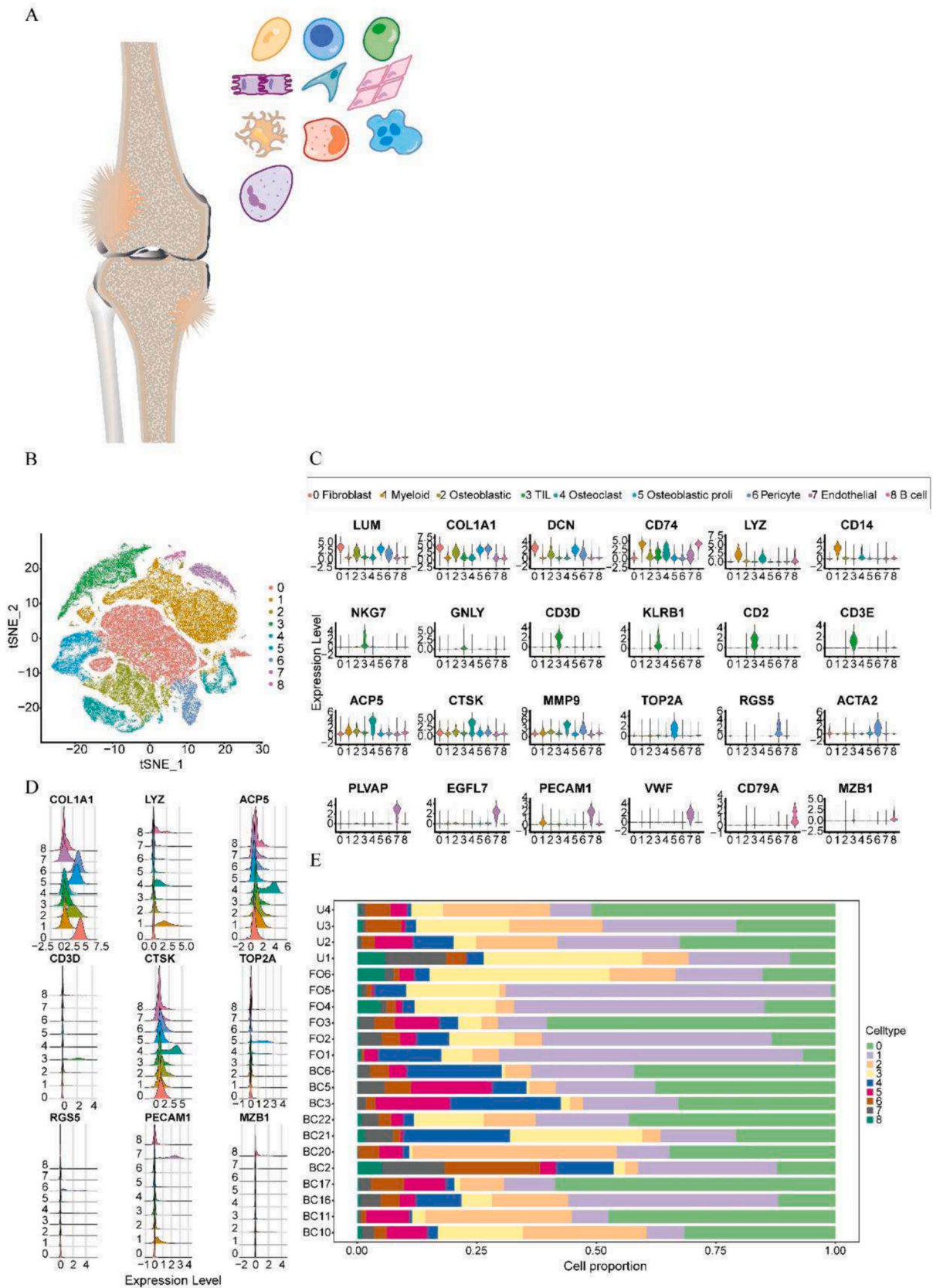


Fig. 1. An overview of integrated bioinformatics analysis of single-cell transcriptome of OS. (A) A total of 134,579 cells were clustered into nine different cell types, including fibroblasts, myeloid cells, osteoblasts, TIL, osteoclasts, proliferative osteoblasts, pericytes, endothelial cells, and B cells. (B) t-SNE analysis was used to identify the nine main OS cell subpopulations. (C–D) Marker genes for each cell cluster were shown. (E) Proportions of each cell cluster in the OS sample were identified pre- and post-chemotherapy. OS sample pre-chemotherapy: U1–U4, FO1–FO6. OS sample post-chemotherapy: BC2, 3, 5, 6, 10, 11, 16, 17, 20, 21, 22. OS, osteosarcoma; TILs, tumor-infiltrating lymphocytes.

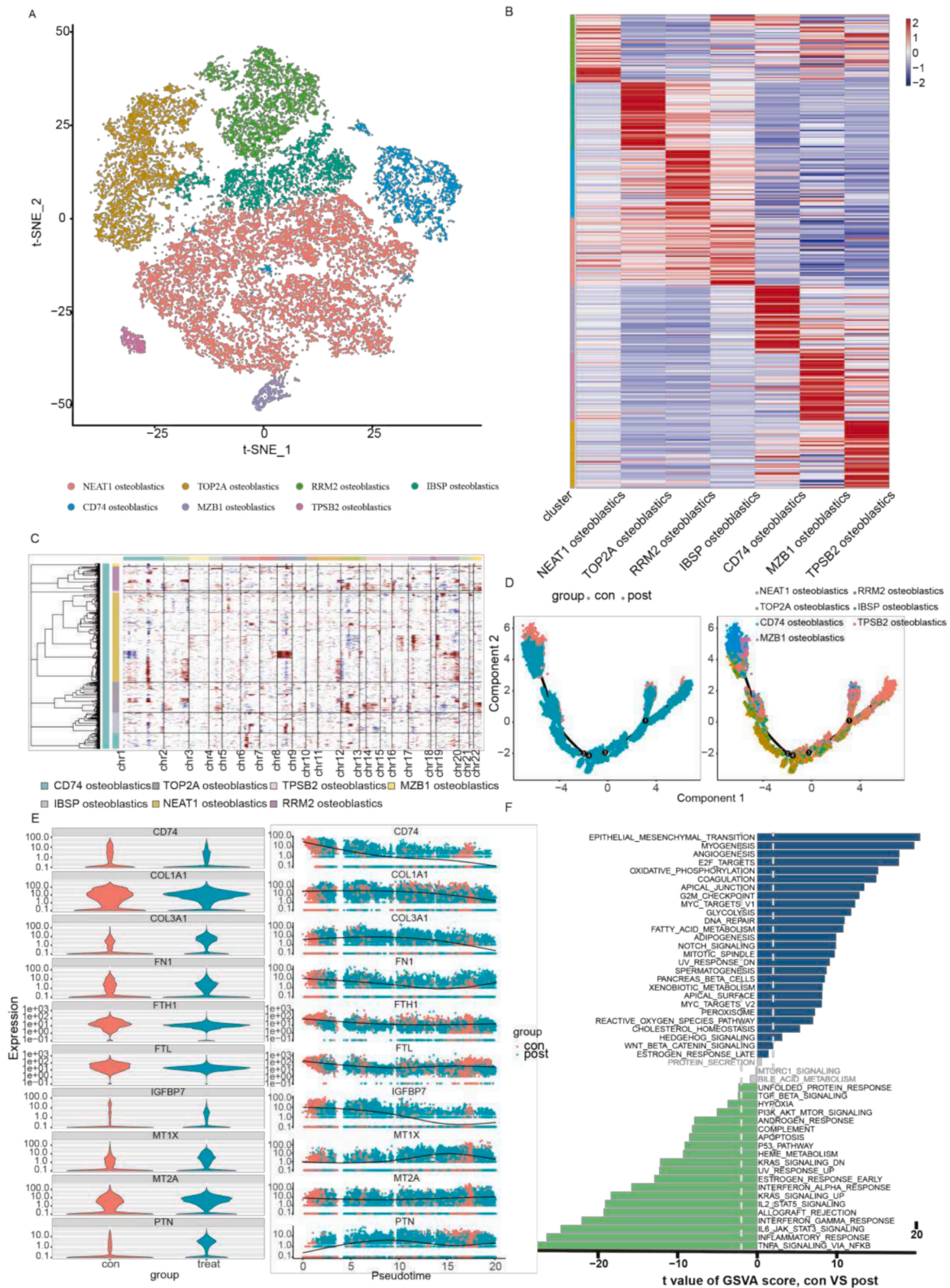


Fig. 2. The osteoblast repopulation and expression patterns in OS. (A) t-SNE was used to demonstrate OS cell subtypes. (B) The heatmap showed the representative marker genes of osteoblast subpopulations, with color gradients from blue to red indicating relative expression levels from low to high. (C) A stratified heatmap displayed CNV characteristics of osteoblast subtypes. The Y axis indicated the different subtypes of osteoblasts; and the X axis represented the various chromosomes, with different colors at the top of the diagram indicating a chromosome. (D) Proposed chronological analysis trajectories of osteoblast subtypes were inferred by Monocle 2 pre- and post-chemotherapy, with each point corresponding to one cell. (E) Pseudotime series analysis trajectories and cell proportion analysis were performed for mono-clonal evolution genes, differential genes and intersection genes pre- and post-chemotherapy. (F) The comparison was conducted among osteoblast enrichment hallmark signaling pathways pre- and post-chemotherapy based on GSEA enrichment scores from the MSigDB database. OS, osteosarcoma; CNV, single-cell copy-number variation; GSEA, gene set variation analysis. (For interpretation of the references to color in this figure legend, the reader is referred to the web version of this article.)

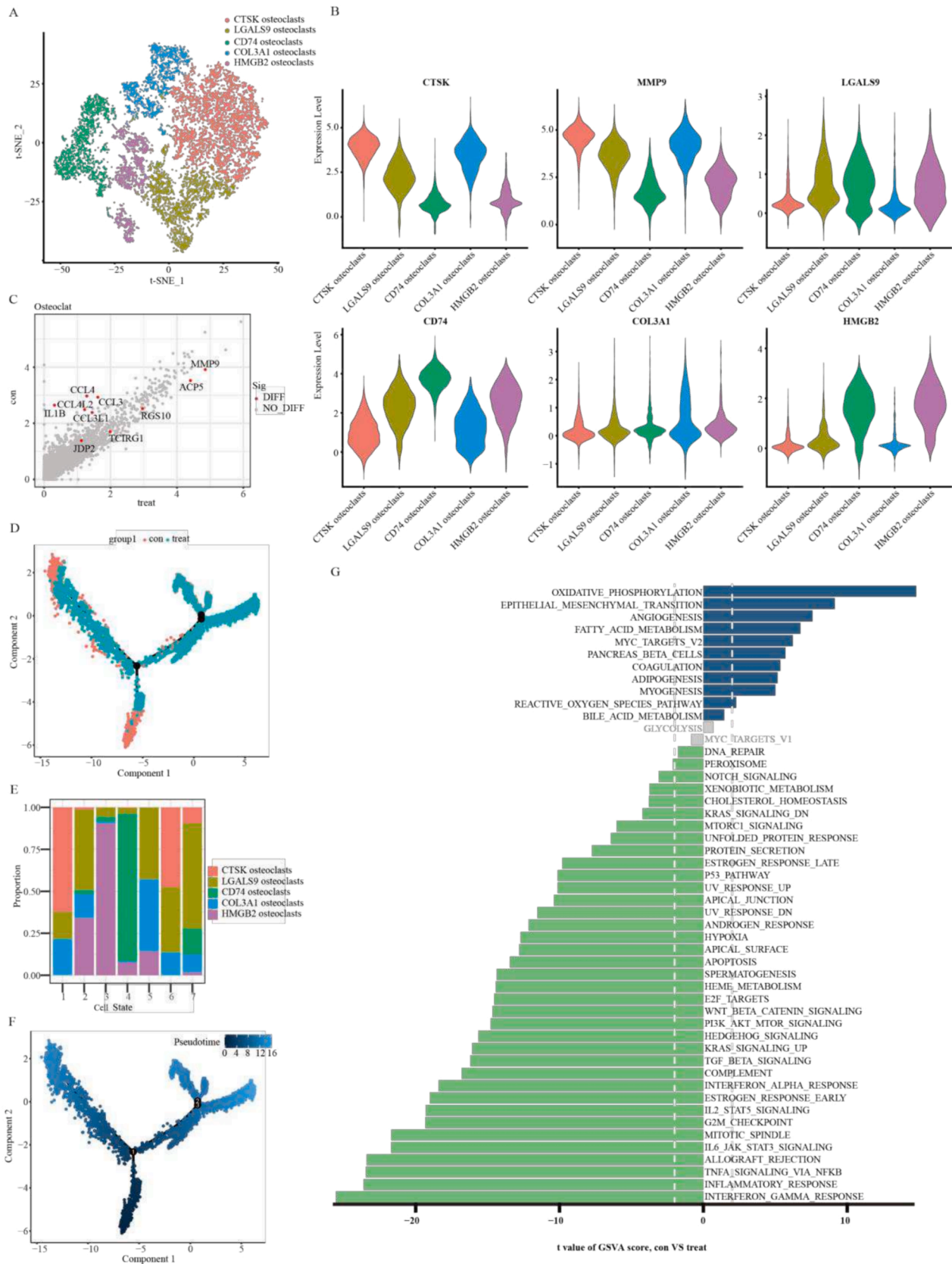


Fig. 3. Cell clustering and functional annotation of osteoclasts in OS lesions. (A) t-SNE was utilized to prove the subpopulation cell types of osteoclast in OS. (B) The violin plot displayed the representative marker genes of the osteoclast subpopulation. (C) The DEGs in patients with OS pre- and post-chemotherapy were presented in a volcano map. (D–F) Monocle 2 trajectory plots exhibited osteoclast cell subpopulation changes post-chemotherapy. (G) GSEA analysis revealed the enrichment of the hallmark signaling pathway of osteoclast post-chemotherapy. OS, osteosarcoma; DEGs, differential expression genes; GSEA, gene set variation analysis.

Post-chemotherapy GSVA analysis exhibited that an up-regulation was found in coagulation, pancreas beta cells, MYC targets v2, fatty acid metabolism, angiogenesis, epithelial-mesenchymal transition, oxidative phosphorylation, while a down-regulation was observed in interferon gamma response, inflammatory response, TNF- α signaling via NF- κ B, allograft rejection, IL6/Jak/Stat3 signaling, mitotic spindle, G2M checkpoint, IL2-STAT5 signaling, and estrogen response early (Fig. 3G).

3.4. Chemotherapy activates the SPP1 cancer-associated fibroblast population

Cancer-associated fibroblast (CAF), an important component of the TME, can stimulate OS progression, growth, and metastasis. t-SNE was used to classify CAF into SPP1 fibroblasts (30,010), IGFBP4 fibroblasts (5,964) and COL10A fibroblasts (4,514) (Fig. 4A–B). Subsequently, we analyzed the effect of chemotherapy on DEGs of CAF, identifying 235 down-regulated DEGs and 244 up-regulated DEGs. The top 10 genes were selected for demonstration (Fig. 4C). To further clarify the effect of chemotherapy on CAF, this study discovered that post-chemotherapy intervention, COL10A fibroblasts evolved into SPP1 fibroblasts and IGFBP4 fibroblasts. The biological functions of SPP1 fibroblasts and IGFBP4 fibroblasts were similar to ossification, endochondral bone morphogenesis, endochondral ossification, replacement ossification, biomineral tissue development, and biomineralization, and correlated with negative regulation of cell motility, negative regulation of cellular component movement, collagen-containing extracellular matrix (ECM), endoplasmic reticulum lumen, and ECM structural constituent (Fig. 4D). Subsequently, branching heat maps were used to present the gene patterns of different cell fate branches. Consistent with the DEGs expression trends, FOS, JUN and HSPA1A were down-regulated post-chemotherapeutic intervention, while COL3A1, COL6A2 and IGFBP7 were up-regulated (Fig. 4E, Supplementary Fig. 4). Based on the pooled CNV results, SPP1 fibroblasts showed increased CNVs on chromosome 1, chromosome 2, chromosome 4 and chromosome 8, and might also play an osteoblast-like function (Fig. 4F).

3.5. Heterogeneity of tumor macrophages and dendritic cells

Tumor-infiltrating myeloid cells, a class of cells, play a key role in TME. Such cells can stimulate and inhibit tumor activity. The descending clustering of myeloid t-SNE was divided into SELENOP macrophages (6,634), FABP5 macrophages (5,330), CCL4L2 macrophages (5,290), neutrophil (2,840), IFIT1 macrophages (2,184), CCL4 macrophages (2,107), CD14 monocytes (2,061), IL7R macrophages (2,048), CSTB macrophages (1,836), COL1A1 macrophages (1,507), and CD1C DCs (1,136) (Fig. 5A–B). Next, after comparing the differential genes in 11 cell subpopulations pre- and post-chemotherapy, the results displayed that 22 genes were up-regulated and 1 gene was down-regulated in SELENOP macrophages; 6 genes up-regulated and 12 genes down-regulated in FABP5 macrophages; 17 genes up-regulated and 12 genes down-regulated in CCL4L2 macrophages; 8 genes up-regulated and 11 genes down-regulated in neutrophil; 8 genes up-regulated and 12 genes down-regulated in IFIT1 macrophages; 23 genes up-regulated and 2 genes down-regulated in CCL4 macrophages; 1 gene up-regulated and 4 genes down-regulated in CD14 monocytes; 4 genes up-regulated and 7 genes down-regulated in IL7R macrophages; 9 genes up-regulated and 3 genes down-regulated in CSTB macrophages; 34 genes up-regulated and 10 genes down-regulated in COL1A1 macrophages; and 1 gene down-regulated in CD1C DCs (Fig. 5C). The proposed time series and cell proportion analysis revealed that post-chemotherapy, the proportion of CD14 monocytes was decreased ($P = 0.03$), while there was an increase in the proportions of SELENOP macrophages ($P = 0.06$), IL7R macrophages ($P = 0.03$), COL1A1 macrophages ($P = 0.03$) and CD1C DCs ($P = 0.07$) (Fig. 5D–E, Supplementary Fig. 5).

Additionally, in this study, the expression of most signaling pathways was decreased by chemotherapy in myeloid cells, such as inflammatory

response, TNF- α signaling via NF- κ B, IL6/Jak/Stat3 signaling, KRAS signaling up, complement, IL2-STAT5 signaling, TGF beta signaling, estrogen response early, apoptosis, androgen response, mitotic spindle, allograft rejection, heme metabolism, interferon gamma response, UV response up, apical junction, PI3K/AKT/mTOR signaling, hypoxia, hedgehog signaling, protein secretion, and P53 pathway. However, only KRAS signaling DN, pancreas beta cells, and spermatogenesis were highly expressed post-chemotherapy (Fig. 5F).

3.6. Chemotherapy reduces Treg cells and NK cells and increases the proportions of CD4+ and CD8+ cell populations

TILs, as key role cells in tumor immunotherapy, have become a hot topic in OS research due to their different cell type composition. In this study, t-SNE was utilized to classify TILs into CD4+ T cells (5,662), CD8+ T cells (5,017), NK cells (1,074), Tregs (1,133) and CD1C-/CD141- DCs (388) (Fig. 6A–B). Post-chemotherapy treatment, the proportions of CD4+ T cells and CD8+ T cells were increased, while the proportions of Tregs, NK cells and CD1C-/CD141- DCs were decreased. Correspondingly, the expression of CLIC3 and GZMB was reduced while the expression of LTB expression was elevated. These results hypothesized that chemotherapy for OS might cause the formation of tumor immunosuppression (Fig. 6C–D). Additionally, the Kyoto Encyclopedia of Genes and Genomes enrichment analysis displayed that post-chemotherapy treatment, scRNA-seq DEGs were mainly enriched in proteoglycans in cancer, protein digestion and absorption, PI3K/Akt signaling pathway, human papillomavirus infection, ECM-receptor interaction and AGE-RAGE signaling pathway in diabetic complications (Fig. 6E).

4. Discussion

The development of OS is closely related to its surrounding complex TME. TME is not isolated but is inseparably linked to the microenvironment surrounding the tumor and even to the whole body in time and space [21,22]. TME is a complex system composed of various cells, including highly heterogeneous malignant cells, endothelial cells, immune cells, and other stromal cells [23,24]. As reported in previous studies, innate immune cells (such as macrophages and suppressor cells from bone marrow) and adaptive immune cells (such as T and B cells) are involved in the development of a variety of tumors such as glioblastoma, squamous cell carcinoma of the tongue, and esophageal cancer [25,26]. The interaction between tumor cells and TME determines tumor progression. The immune system plays two distinct roles in tumor development. The immune system, on the one hand, has a natural anti-tumor effect in the early stage of tumor invasion. On the other hand, it exhibits a pro-tumor phenotype during tumor progression, leading to tumor immune escape and metastasis.

Traditional RNA-seq and gene microarrays can only sequence the total RNA of samples, but cannot distinguish differential gene expression in varied cell types. Therefore, the tumorigenesis and progression cannot be resolved by sequencing results [27]. In this study, 10 \times Genomics high-throughput scRNA-seq was used to analyze the characteristics of patients with OS. Besides, we characterized the cellular composition of OS at the single-cell level using specific marker genes and identified nine cell types, including fibroblasts, myeloid cells, osteoblasts, TILs, osteoclasts, proliferative osteoblasts, pericytes, endothelial cells, and B cells. Subsequently, inferCNV, proposed time series analysis, and GSVA were used to analyze the differential changes in cell subtypes pre- and post-chemotherapy. Interestingly, a decrease was presented in the proportions of myeloid cells and TILs, while an increase was found in the number of osteoblasts. Furthermore, there was a reduction in the proportions of CD14 monocytes, Tregs, NK cells and CD1C-/CD141-DCs, whereas there was an elevation in the proportions of SELENOP macrophages, IL7R macrophages, COL1A1 macrophages, CD1C DCs, CD4+ T cells and CD8+ T cells. Such results were consistent with previous

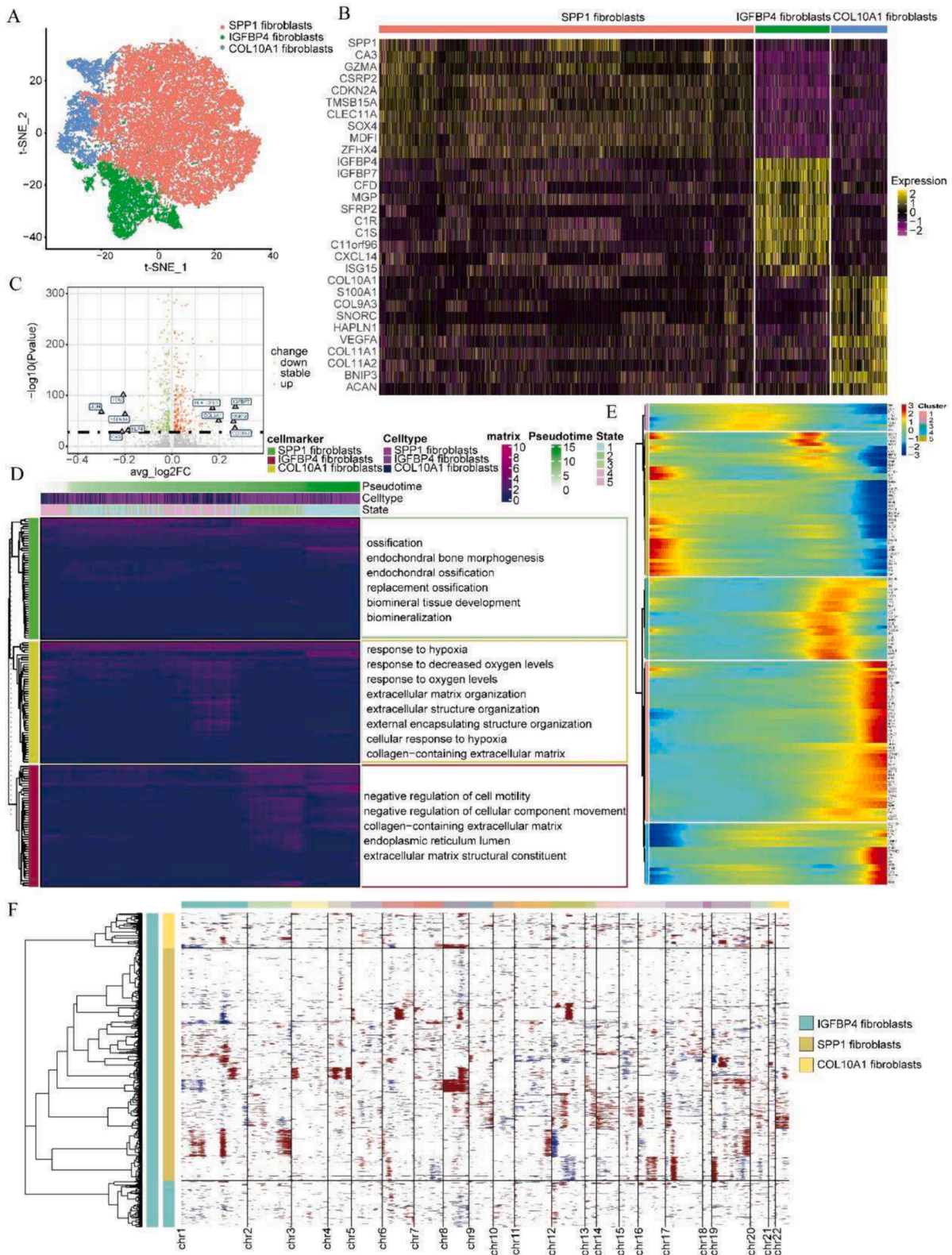


Fig. 4. Changes in fibroblast structure and gene expression profiles in the TME of OS post-chemotherapy treatment. (A) t-SNE was performed to show the subpopulation cell types of osteoclasts in OS. (B) The heat map revealed representative marker genes of fibroblast subpopulations, with color gradients from purple to yellow indicating relative expression levels from low to high. (C) The volcano plot displayed the upregulated and downregulated DEGs post-chemotherapy. (D) Monocle 2 in the hierarchical clustering diagram was inferred by pseudotime trajectory and KEGG signaling pathway enrichment of fibroblasts post-chemotherapeutic intervention. (E) The OS-related gene expression post-chemotherapy was presented in a heat map. The color key from blue to red indicated the relative expression levels from low to high. (F) The stratified heat map exhibited the changes in CNV of different fibroblast types. Different colors at the top of the diagram indicated a chromosome. TME, tumor microenvironment; OS, osteosarcoma; KEGG, Kyoto Encyclopedia of Genes and Genomes; CNV, single-cell copy-number variation. (For interpretation of the references to color in this figure legend, the reader is referred to the web version of this article.)

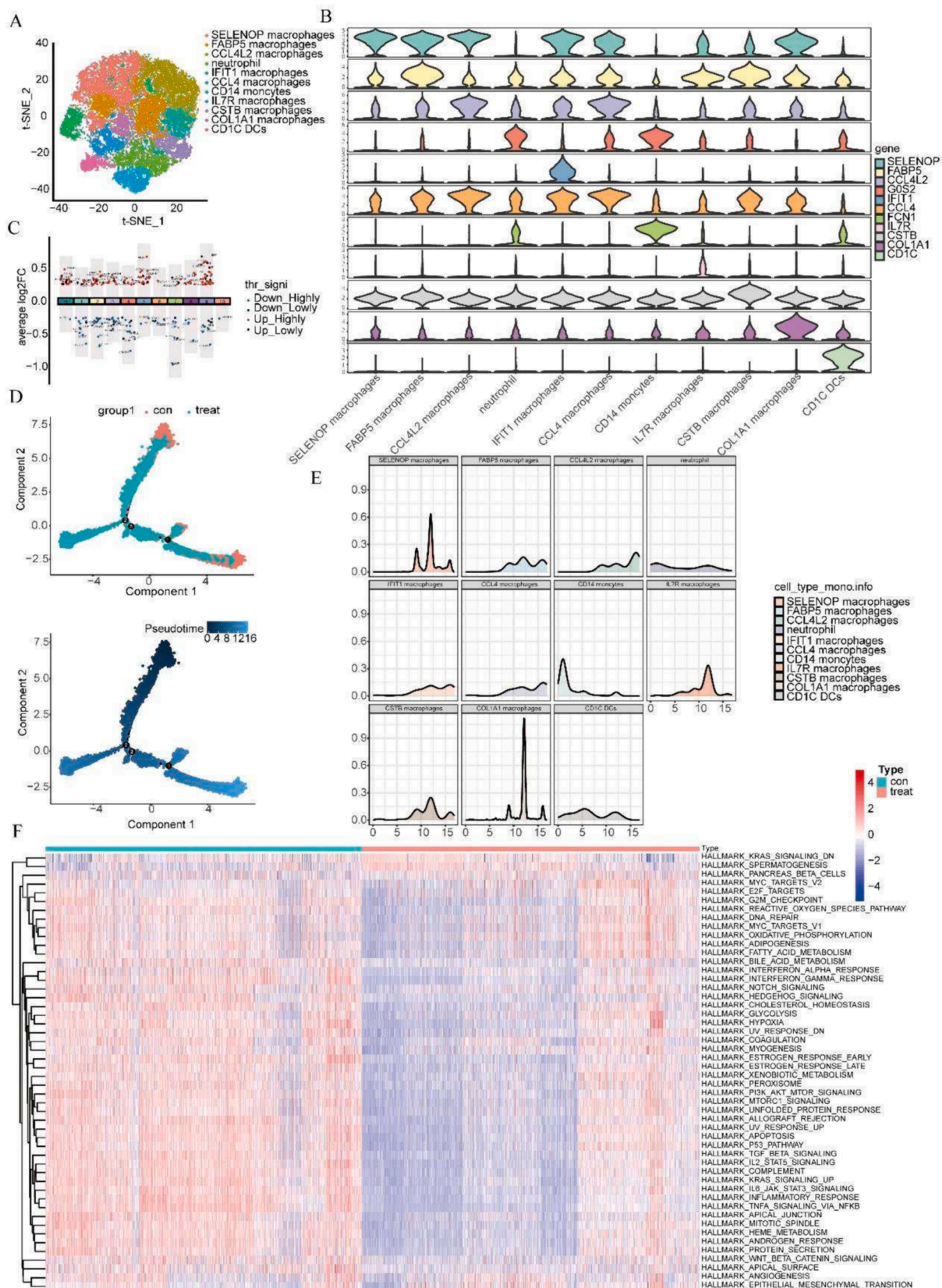
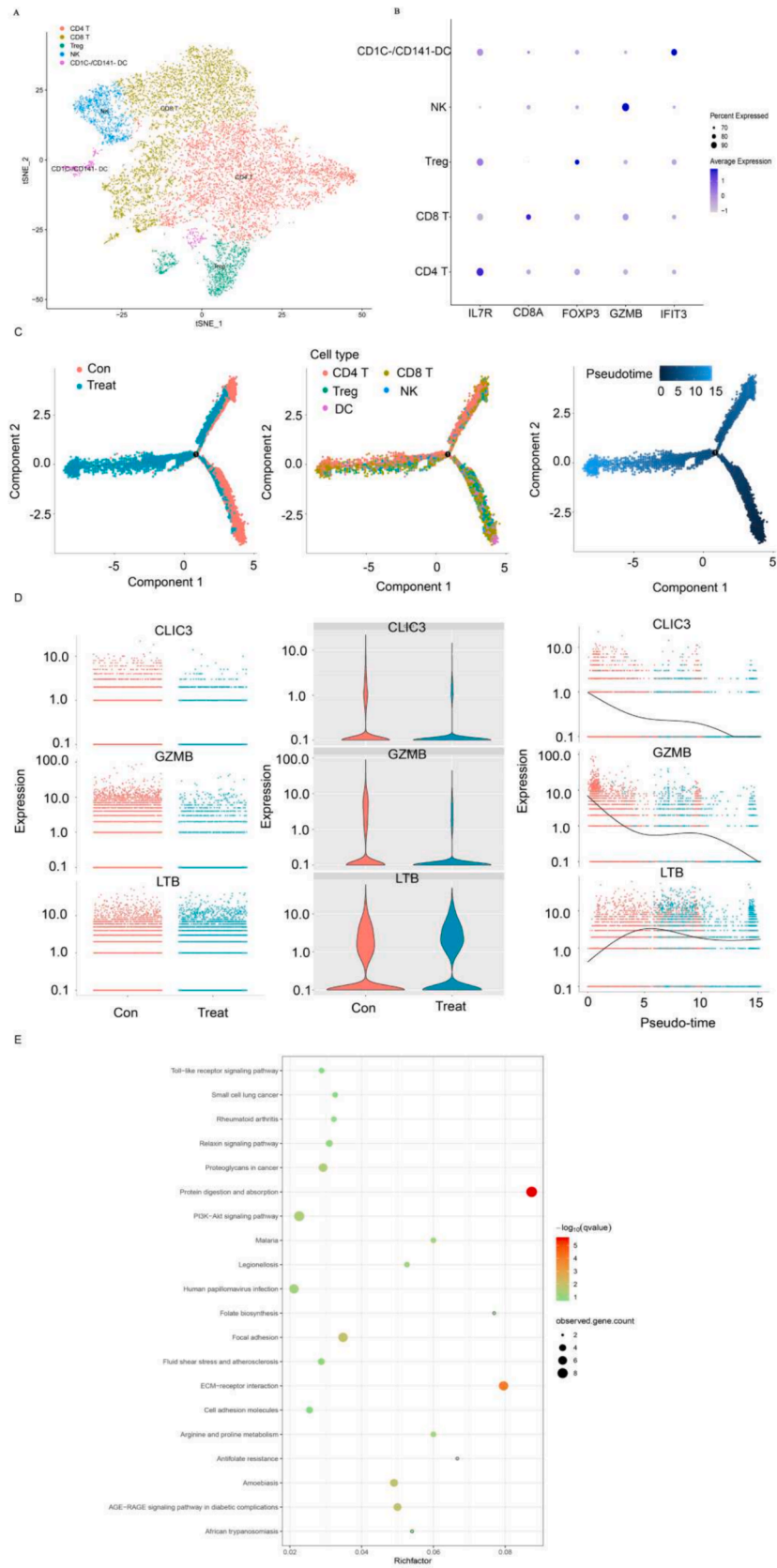


Fig. 5. Clustering and identification of myeloid cells post-chemotherapy. (A) t-SNE was used to identify the cell types of myeloid cells in OS. (B) The violin plot displayed representative marker genes of myeloid cell subpopulations. (C) The DEGs were up-regulated and down-regulated in myeloid cells post-chemotherapy. (D) The proposed chronological analysis of trajectories of myeloid cells was inferred by Monocle 2. (E) The effects of chemotherapy on the proportions of myeloid cell subtypes were analyzed. The y-axis represented the proportions of myeloid cell subtypes; the x-axis indicated pseudotime. (F) The heat map revealed the enrichment of the hallmark signaling pathway in myeloid cells. OS, osteosarcoma; DEGs, differentially expressed genes.



(caption on next page)

Fig. 6. Cell types, functional characteristics and proportions of key cell subtype of TILs in the OS TME post-chemotherapy. (A) t-SNE was applied to analyze the subpopulation of TIL cells from patients with OS. (B) Bubble plots showed the representative marker genes for cell subpopulations of TILs, with color gradients from gray to blue indicating the relative expression levels from low to high. (C) Proposed chronological analysis trajectories of TILs were inferred by Monocle 2, with each point corresponding to one cell. (D) The plot exhibited the trajectories of proposed chronological changes in TIL characteristics of patients with OS post-chemotherapeutic intervention. (E) The bubble plot reviewed the enrichment of the KEGG signaling pathway of TILs DEGs post-chemotherapy. TILs, tumor-infiltrating lymphocytes; OS, osteosarcoma; TME, tumor microenvironment; KEGG, Kyoto Encyclopedia of Genes and Genomes; DEGs, differentially expressed genes. (For interpretation of the references to color in this figure legend, the reader is referred to the web version of this article.)

studies. As demonstrated by Liu et al., the scarce presence of CD8⁺ T cells was confirmed in untreated OS tissues through ScRNA-seq [28]. Similarly, based on the results of He et al. [29], patients with OS undergoing metastasis post-neoadjuvant chemotherapy exhibited low levels of CD8⁺ T cells via ScRNA-seq. Combined with the increased proportion of CD8⁺ T cells post-chemotherapy observed in this study, it is suggested that CD8⁺ T cells could serve as potential targets for immunotherapy.

OS is a common malignant bone tumor. Despite being sensitive to certain chemotherapeutic agents, it may develop chemoresistance in cancer cells during treatment [30]. Although the use of neoadjuvant chemotherapy has had a dramatic impact on the overall survival of patients with OS, there has been no significant improvement over the past 30 years. Besides, patients with metastatic and recurrent OS have an even worse prognosis, with a 5-year overall survival rate of only 20 % [2,31,32]. Currently, the main chemotherapeutic agents for OS are methotrexate, doxorubicin, and platinum-based drugs [33,34].

TME is a microenvironment consisting of multiple cell types (fibroblasts, endothelial cells and immune cells), extracellular components (chemokines, cytokines, ECM, etc.) and physical and chemical factors (hypoxia, and acidity) surrounding the tumor [35]. TME plays a crucial role in tumor development. The non-tumor cells are more susceptible to higher genetic variation because the genetic variation of non-tumor cells in TME was smaller than tumor cells, thus leading to chemoresistance [36,37]. In this study, the investigation on osteoblastic and osteoclast cells confirmed that CD74, FTL, FTH1, MT1X and MT2A were down-regulated post-chemotherapy, while PTN, COL3A1, COL1A1, IGFBP7 and FN1 were up-regulated. Meanwhile, EMT, DNA repair, G2M checkpoint, and E2F targets were highly enriched post-chemotherapy, and MMP9 was highly expressed in CTSK osteoclasts, LGALS9 osteoclasts, and COL3A1 osteoclasts. Not surprisingly, tumor macrophages can promote EMT and up-regulate MMP-9 in OS cells post-chemotherapy intervention, thus facilitating chemoresistance [38].

Additionally, CNV changes were observed in CAF in this study, suggesting that TME cells are not merely receptive to cancer cells, but are passively involved in tumorigenesis. Genetic variation does not occur only in tumor cells, but extensively in non-epithelial TME cells. This occurrence of irreversible and permanent genetic variation may further contribute to tumorigenesis. An integrin binding glycoprotein, called osteopontin, was encoded by the SPP1 gene [39,40]. It is secreted by various tumors and is associated with tumor progression, invasion and metastasis. The expression of SPP1 is significantly associated with TAMs in multiple tumors, although it may act as a chemokine that recruits macrophages. However, according to a recent study, CAF-derived SPP1 can promote EMT via the integrin-protein kinase C- α signaling pathway, thereby activating fibrosarcoma/mitogen-activated protein kinase and phosphatidylinositol 3-kinase /protein kinase B/mammalian target of rapamycin. However, SPP1 inhibitors can promote EMT and reverse CAF-induced resistance to tyrosine kinase inhibitors *in vivo* [41]. The above results suggest that targeting SPP1 CAF may be a breakthrough in immunotherapy resistance in patients with OS, and contribute to deepening the understanding of chemoresistance in OS.

Furthermore, this study revealed that the proportions of Tregs and NK cells were decreased and the ratio of CD138 DCs was increased post-chemotherapy treatment. Treg cells typically participate in suppressing immune responses to promote tumor tolerance, and their reduction might initially suggest a decreased immunosuppressive environment.

The loss of NK cells can significantly impair the ability of TME to initiate effective anti-tumor immune responses. These phenomena suggest that OS chemotherapy can cause the formation of an immunosuppressive TME, possibly contributing to the development of OS. Besides, OS chemotherapy plays a role in the development of drug resistance by promoting tumor immune escape, deterioration, increasing invasiveness, and antagonizing treatments [42–44].

Overall, in this study, the different cell types of OS were analyzed using scRNA-seq and the different cell clusters were annotated using the cell indication marker. The relationship between osteoclasts and OS development has been illustrated. Most importantly, this study provided novel insights into the effects of chemotherapy on OS cell subtypes by analyzing the differences in OS cell landscape pre- and post-chemotherapy, offering significant support to discover new therapeutic targets for OS and investigate the therapeutic approaches for OS. Therefore, the studies on the OS landscape were expected to discover new therapeutic targets and improve OS therapeutic approaches.

There are some limitations in this study. First, the number of sample cases is small due to the rarity of patients with OS and the lack of normal controls. Second, we analyzed the differences in biological functions and cell-to-cell interactions for each of the nine major cell types/subtypes using a cell marker. Third, the expression of long-stranded non-coding RNAs in OS has been identified in some recent scRNA-seq studies [45,46]. These findings contribute to further explaining the molecular mechanism of OS, which is yet to be explored. Finally, the actual expression of DEGs screened in this study has not been verified by RT-qPCR or western blot, nor was there an in-depth exploration of their possible regulatory mechanisms. It is not available to comprehensively describe all cell types, subtypes and phenotypes in one report, and more comprehensive and deeper studies will be further investigated in the future.

CRediT authorship contribution statement

Xiao-yu He: Writing – review & editing, Writing – original draft, Visualization, Validation, Supervision, Software, Resources, Project administration, Methodology, Investigation, Funding acquisition, Formal analysis, Data curation, Conceptualization. **Liu-yi Que:** Validation, Software, Project administration, Methodology, Investigation, Formal analysis, Data curation. **Fan Yang:** Supervision, Software, Project administration, Investigation, Data curation, Conceptualization. **Yi Feng:** Resources, Project administration, Methodology, Funding acquisition, Formal analysis, Data curation. **Dong Ren:** Visualization, Validation, Software, Resources, Methodology. **Xiang Song:** Writing – review & editing, Writing – original draft, Visualization, Validation, Supervision, Software, Resources, Project administration, Methodology, Investigation, Funding acquisition, Formal analysis, Data curation, Conceptualization.

Declaration of competing interest

The authors declare that they have no known competing financial interests or personal relationships that could have appeared to influence the work reported in this paper.

Acknowledgements

Not applicable.

Authors' contributions

XH conceived and designed the study, and drafted the initial manuscript. LQ, FY, YF and DR collected the data and carried out the initial analyses. XS critically reviewed the manuscript for important intellectual content. All authors approved the final manuscript for submission and agreed to be accountable for all aspects of the work.

Funding

This study is supported by the Shanxi Provincial Science and Technology Department (grant 201904D131029).

Availability of data and materials

The data used to support the findings of this study are available from the corresponding author upon request.

Ethics approval and consent to participate

This study was approved by the Ethics Committee of the Second Hospital of Shanxi Medical University (2022YX NO.168) and complied with all relevant ethical regulations. All patients with OS provided written informed consent.

Appendix A. Supplementary data

Supplementary data (Supplementary Fig. 1: Differences in principal component analysis grouping and cell group proportions pre- and post-chemotherapy for osteosarcoma. Red indicated pre-chemotherapy and blue represented post-chemotherapy. The t-test was used to analyze the differences between the two groups. Supplementary Fig. 2: Osteoblast differential genes and proposed chronological analysis of intersection genes in osteosarcoma. Supplementary Fig. 3: Pseudotime trajectory analysis of osteoclast subtypes in osteosarcoma. Supplementary Fig. 4: Pseudo-chronological analysis of gene changes and co-expressed genes of differential genes in fibroblasts pre- and post-chemotherapy intervention. Supplementary Fig. 5: Effect of chemotherapy on the proportion of different subtypes of macrophages in osteosarcoma.) to this article can be found online at <https://doi.org/10.1016/j.jbo.2024.100604>.

References

- [1] P.S. Meltzer, L.J. Helman, New horizons in the treatment of osteosarcoma, *N. Engl. J. Med.* 385 (22) (2021) 2066–2076.
- [2] Z. Shoaib, T.M. Fan, J.M.K. Irudayaraj, Osteosarcoma mechanobiology and therapeutic targets, *Br. J. Pharmacol.* 179 (2) (2022) 201–217.
- [3] Y. Chen, R. Liu, W. Wang, C. Wang, N. Zhang, X. Shao, Q. He, M. Ying, Advances in targeted therapy for osteosarcoma based on molecular classification, *Pharmacol. Res.* 169 (2021) 105684.
- [4] C.A. Stiller, S.S. Bielack, G. Jundt, E. Steliarova-Foucher, Bone tumours in European children and adolescents, 1978–1997. Report from the automated childhood cancer information system project, *Eur. J. Cancer (Oxford, England: 1990)* 42(13) (2006) 2124–2135.
- [5] S.S. Bielack, B. Kempf-Bielack, G. Dellling, G.U. Exner, S. Flege, K. Helmke, R. Kotz, M. Salzer-Kuntschik, M. Werner, W. Winkelmann, A. Zoubek, H. Jürgens, K. Winkler, Prognostic factors in high-grade osteosarcoma of the extremities or trunk: an analysis of 1,702 patients treated on neoadjuvant cooperative osteosarcoma study group protocols, *J. Clin. Oncol.* 20 (3) (2002) 776–790.
- [6] L. Mirabello, R.J. Troisi, S.A. Savage, Osteosarcoma incidence and survival rates from 1973 to 2004: data from the Surveillance, epidemiology, and end results program, *Cancer* 115 (7) (2009) 1531–1543.
- [7] D.C. Dahlin, K.K. Unni, Osteosarcoma of bone and its important recognizable varieties, *Am. J. Surg. Pathol.* 1 (1) (1977) 61–72.
- [8] B. Celik, K. Cicek, A.F. Leal, S. Tomatsu, Regulation of molecular targets in osteosarcoma treatment, *Int. J. Mol. Sci.* 23 (20) (2022).
- [9] Y. Wen, F. Tang, C. Tu, F. Hornicek, Z. Duan, L. Min, Immune checkpoints in osteosarcoma: Recent advances and therapeutic potential, *Cancer Lett.* 547 (2022) 215887.
- [10] J. Gill, R. Gorlick, Advancing therapy for osteosarcoma, *Nat. Rev. Clin. Oncol.* 18 (10) (2021) 609–624.
- [11] J. Liang, W. Cai, Z. Sun, Single-cell sequencing technologies: current and future, *J. Genet. Genom. = Yi Chuan Xue Bao* 41 (10) (2014) 513–528.
- [12] X. Huang, L. Wang, H. Guo, W. Zhang, Z. Shao, Single-cell transcriptomics reveals the regulative roles of cancer associated fibroblasts in tumor immune microenvironment of recurrent osteosarcoma, *Theranostics* 12 (13) (2022) 5877–5887.
- [13] Y. Zhou, D. Yang, Q. Yang, X. Lv, W. Huang, Z. Zhou, Y. Wang, Z. Zhang, T. Yuan, X. Ding, L. Tang, J. Zhang, J. Yin, Y. Huang, W. Yu, Y. Wang, C. Zhou, Y. Su, A. He, Y. Sun, Z. Shen, B. Qian, W. Meng, J. Fei, Y. Yao, X. Pan, P. Chen, H. Hu, Single-cell RNA landscape of intratumoral heterogeneity and immunosuppressive microenvironment in advanced osteosarcoma, *Nat. Commun.* 11 (1) (2020) 6322.
- [14] M. Armaka, D. Konstantopoulos, C. Tzaferis, M.D. Lavigne, M. Sakkou, A. Liakos, P. P. Sfrikakis, M.A. Dimopoulos, M. Fousteri, G. Kollias, Single-cell multimodal analysis identifies common regulatory programs in synovial fibroblasts of rheumatoid arthritis patients and modeled TNF-driven arthritis, *Genome Med.* 14 (1) (2022) 78.
- [15] H. Shao, M. Ge, J. Zhang, T. Zhao, S. Zhang, Osteoclasts differential-related prognostic biomarker for osteosarcoma based on single cell, bulk cell and gene expression datasets, *BMC Cancer* 22 (1) (2022) 288.
- [16] Z. Zeng, W. Li, D. Zhang, C. Zhang, X. Jiang, R. Guo, Z. Wang, C. Yang, H. Yan, Z. Zhang, Q. Wang, R. Huang, Q. Zhao, B. Li, X. Hu, L. Gao, Development of a chemoresistant risk scoring model for prechemotherapy osteosarcoma using single-cell sequencing, *Front. Oncol.* 12 (2022) 893282.
- [17] X. Zhang, Y. Lan, J. Xu, F. Quan, E. Zhao, C. Deng, T. Luo, L. Xu, G. Liao, M. Yan, Y. Ping, F. Li, A. Shi, J. Bai, T. Zhao, X. Li, Y. Xiao, Cell Marker: a manually curated resource of cell markers in human and mouse, *Nucleic Acids Res.* 47 (D1) (2019) D721–D728.
- [18] O. Franzén, L.M. Gan, J.L.M. Björkegren, PanglaoDB: a web server for exploration of mouse and human single-cell RNA sequencing data, *Database (Oxford)* 2019 (2019).
- [19] A.A. Ionkina, G. Balderrama-Gutierrez, K.J. Ibanez, S.H.D. Phan, A.N. Cortez, A. Mortazavi, J.A. Prescher, Transcriptome analysis of heterogeneity in mouse model of metastatic breast cancer, *Breast Cancer Res.: BCR* 23 (1) (2021) 93.
- [20] A. Liberzon, C. Birger, H. Thorvaldsdóttir, M. Ghandi, J.P. Mesirov, P. Tamayo, The Molecular Signatures Database (MSigDB) hallmark gene set collection, *Cell Syst.* 1 (6) (2015) 417–425.
- [21] M.F. Heymann, F. Lézot, D. Heymann, The contribution of immune infiltrates and the local microenvironment in the pathogenesis of osteosarcoma, *Cell. Immunol.* 343 (2019) 103711.
- [22] R.T. Netea-Maier, J.W.A. Smit, M.G. Netea, Metabolic changes in tumor cells and tumor-associated macrophages: A mutual relationship, *Cancer Lett.* 413 (2018) 102–109.
- [23] C. Zhang, J.H. Zheng, Z.H. Lin, H.Y. Lv, Z.M. Ye, Y.P. Chen, X.Y. Zhang, Profiles of immune cell infiltration and immune-related genes in the tumor microenvironment of osteosarcoma, *Aging* 12 (4) (2020) 3486–3501.
- [24] C. Genova, C. Dellepiane, P. Carrega, S. Sommariva, G. Ferlazzo, P. Pronzato, R. Gangemi, G. Filaci, S. Coco, M. Croce, Therapeutic implications of tumor microenvironment in lung cancer: focus on immune checkpoint blockade, *Front. Immunol.* 12 (2021) 799455.
- [25] Y. Liu, X. Li, Y. Zhang, H. Wang, X. Rong, J. Peng, L. He, Y. Peng, An miR-340-5p-macrophage feedback loop modulates the progression and tumor microenvironment of glioblastoma multiforme, *Oncogene* 38 (49) (2019) 7399–7415.
- [26] S. Kimura, U. Nanbu, H. Noguchi, Y. Harada, K. Kumamoto, Y. Sasaguri, T. Nakayama, Macrophage CCL22 expression in the tumor microenvironment and implications for survival in patients with squamous cell carcinoma of the tongue, *J. Oral Pathol. Med.* 48 (8) (2019) 677–685.
- [27] M. Su, T. Pan, Q.Z. Chen, W.W. Zhou, Y. Gong, G. Xu, H.Y. Yan, S. Li, Q.Z. Shi, Y. Zhang, X. He, C.J. Jiang, S.C. Fan, X. Li, M.J. Cairns, X. Wang, Y.S. Li, Data analysis guidelines for single-cell RNA-seq in biomedical studies and clinical applications, *Mil. Med. Res.* 9 (1) (2022) 68.
- [28] Y. Liu, W. Feng, Y. Dai, M. Bao, Z. Yuan, M. He, Z. Qin, S. Liao, J. He, Q. Huang, Z. Yu, Y. Zeng, B. Guo, R. Huang, R. Yang, Y. Jiang, J. Liao, Z. Xiao, X. Zhan, C. Lin, J. Xu, Y. Ye, J. Ma, Q. Wei, Z. Mo, Single-cell transcriptomics reveals the complexity of the tumor microenvironment of treatment-naive osteosarcoma, *Front. Oncol.* 11 (2021) 709210.
- [29] M. He, X. Jiang, J. Miao, W. Feng, T. Xie, S. Liao, Z. Qin, H. Tang, C. Lin, B. Li, J. Xu, Y. Liu, Z. Mo, Q. Wei, A new insight of immunosuppressive microenvironment in osteosarcoma lung metastasis, *Exp. Biol. Med. (Maywood)* 248 (12) (2023) 1056–1073.
- [30] J.A. Lee, J. Lim, H.Y. Jin, M. Park, H.J. Park, J.W. Park, J.H. Kim, H.G. Kang, Y. J. Won, Osteosarcoma in adolescents and young adults, *Cells* 10 (10) (2021).
- [31] C. Chen, L. Xie, T. Ren, Y. Huang, J. Xu, W. Guo, Immunotherapy for osteosarcoma: Fundamental mechanism, rationale, and recent breakthroughs, *Cancer Lett.* 500 (2021) 1–10.
- [32] H.C. Beird, S.S. Bielack, A.M. Flanagan, J. Gill, D. Heymann, K.A. Janeway, J. A. Livingston, R.D. Roberts, S.J. Strauss, R. Gorlick, Osteosarcoma, *Nat. Rev. Dis. Primers* 8 (1) (2022) 77.
- [33] Y. Lu, J. Zhang, Y. Chen, Y. Kang, Z. Liao, Y. He, C. Zhang, Novel immunotherapies for osteosarcoma, *Front. Oncol.* 12 (2022) 830546.
- [34] Z. Hu, S. Wen, Z. Huo, Q. Wang, J. Zhao, Z. Wang, Y. Chen, L. Zhang, F. Zhou, Z. Guo, H. Liu, S. Zhou, Current status and prospects of targeted therapy for osteosarcoma, *Cells* 11 (21) (2022).
- [35] M.T. Bilotta, A. Antignani, D.J. Fitzgerald, Managing the TME to improve the efficacy of cancer therapy, *Front. Immunol.* 13 (2022) 954992.

- [36] X. Tong, R. Tang, M. Xiao, J. Xu, W. Wang, B. Zhang, J. Liu, X. Yu, S. Shi, Targeting cell death pathways for cancer therapy: recent developments in necroptosis, pyroptosis, ferroptosis, and cuproptosis research, *J. Hematol. Oncol.* 15 (1) (2022) 174.
- [37] Y. Xu, X. Wang, L. Liu, J. Wang, J. Wu, C. Sun, Role of macrophages in tumor progression and therapy (Review), *Int. J. Oncol.* 60 (5) (2022).
- [38] Y.Y. Jung, C.D. Mohan, S. Rangappa, J.Y. Um, A. Chinnathambi, S.A. Alharbi, K. S. Rangappa, K.S. Ahn, Brucein D imparts a growth inhibitory effect in multiple myeloma cells by abrogating the Akt-driven signaling pathway, *IUBMB Life* 75 (2) (2023) 149–160.
- [39] W. Li, Z. Ding, D. Wang, C. Li, Y. Pan, Y. Zhao, H. Zhao, T. Lu, R. Xu, S. Zhang, B. Yuan, Y. Zhao, Y. Yin, Y. Gao, J. Li, M. Yan, Ten-gene signature reveals the significance of clinical prognosis and immuno-correlation of osteosarcoma and study on novel skeleton inhibitors regarding MMP9, *Cancer Cell Int.* 21 (1) (2021) 377.
- [40] E.Y. Lin, W. Xi, N. Aggarwal, M.L. Shinohara, Osteopontin (OPN)/SPP1: From its biochemistry to biological functions in the innate immune system and the central nervous system CNS, *Int. Immunol.* (2022).
- [41] J.W. Eun, J.H. Yoon, H.R. Ahn, S. Kim, Y.B. Kim, S.B. Lim, W. Park, T.W. Kang, G. O. Baek, M.G. Yoon, J.A. Son, J.H. Weon, S.S. Kim, H.J. Cho, J.Y. Cheong, Cancer-associated fibroblast-derived secreted phosphoprotein 1 contributes to resistance of hepatocellular carcinoma to sorafenib and lenvatinib, *Cancer Commun. (London, England)* (2023).
- [42] C.C. Wu, H.C. Beird, J. Andrew Livingston, S. Advani, A. Mitra, S. Cao, A. Reuben, D. Ingram, W.L. Wang, Z. Ju, C. Hong Leung, H. Lin, Y. Zheng, J. Roszik, W. Wang, S. Patel, R.S. Benjamin, N. Somaiah, A.P. Conley, G.B. Mills, P. Hwu, R. Gorlick, A. Lazar, N.C. Daw, V. Lewis, P.A. Futreal, Immuno-genomic landscape of osteosarcoma, *Nat. Commun.* 11 (1) (2020) 1008.
- [43] W. Liu, H. Hu, Z. Shao, X. Lv, Z. Zhang, X. Deng, Q. Song, Y. Han, T. Guo, L. Xiong, B. Wang, Y. Zhang, Characterizing the tumor microenvironment at the single-cell level reveals a novel immune evasion mechanism in osteosarcoma, *Bone Res.* 11 (1) (2023) 4.
- [44] J. Wang, F. Hu, P. Yu, J. Wang, Z. Liu, Q. Bao, W. Zhang, J. Wen, Sorafenib inhibits doxorubicin-induced PD-L1 upregulation to improve immunosuppressive microenvironment in Osteosarcoma, *J. Cancer Res. Clin. Oncol.* (2022).
- [45] E. Rothzerg, W. Feng, D. Song, H. Li, Q. Wei, A. Fox, D. Wood, J. Xu, Y. Liu, Single-cell transcriptome analysis reveals paraspeckles expression in osteosarcoma tissues, *Cancer Inform.* 21 (2022).
- [46] E. Rothzerg, J. Xu, D. Wood, Identification of differentially expressed intronic transcripts in osteosarcoma, *Noncoding RNA* 8 (6) (2022) 73.